HMGB2 orchestrates the chromatin landscape of senescence-associated secretory phenotype gene loci

Katherine M. Aird,[1] Osamu Iwasaki,[1] Andrew V. Kossenkov,[2] Hideki Tanizawa,[1] Nail Fatkhutdinov,[1,4] Benjamin G. Bitler,[1] Linh Le,[1,5] Gretchen Alicea,[3] Ting-Lin Yang,[6] F. Brad Johnson,[6] Ken-ichi Noma,[1] and Rugang Zhang[1]

[1]Gene Expression and Regulation Program, [2]Center for Systems and Computational Biology, and [3]Tumor Microenvironment and Metastasis Program, The Wistar Institute, Philadelphia, PA 19104
[4]Kazan Federal University, Kazan 42000, Russia
[5]Cell and Molecular Biology Graduate Group and [6]Department of Pathology and Laboratory Medicine, Perelman School of Medicine, University of Pennsylvania, Philadelphia, PA 19014

Cellular senescence is a stable cell growth arrest that is characterized by the silencing of proliferation-promoting genes through compaction of chromosomes into senescence-associated heterochromatin foci (SAHF). Paradoxically, senescence is also accompanied by increased transcription of certain genes encoding for secreted factors such as cytokines and chemokines, known as the senescence-associated secretory phenotype (SASP). How SASP genes are excluded from SAHF-mediated global gene silencing remains unclear. In this study, we report that high mobility group box 2 (HMGB2) orchestrates the chromatin landscape of SASP gene loci. HMGB2 preferentially localizes to SASP gene loci during senescence. Loss of HMGB2 during senescence blunts SASP gene expression by allowing for spreading of repressive heterochromatin into SASP gene loci. This correlates with incorporation of SASP gene loci into SAHF. Our results establish HMGB2 as a novel master regulator that orchestrates SASP through prevention of heterochromatin spreading to allow for exclusion of SASP gene loci from a global heterochromatin environment during senescence.

Introduction

Cellular senescence is defined as a stable cell cycle exit that can be induced by several stimuli, including oncogenes and critically shortened telomeres (Pérez-Mancera et al., 2014; Childs et al., 2015). Oncogene-induced senescence is a bona fide tumor suppressor mechanism, whereas senescence caused by shortened telomeres (replicative senescence) is known to play a role in tissue aging (Campisi et al., 2011; Campisi, 2013). Senescence is often accompanied by an increase in the expression of secreted factors such as cytokines and chemokines, which is termed the senescence-associated secretory phenotype (SASP; Pérez-Mancera et al., 2014). The SASP is regulated in part through nuclear factor κB (NF-κB) and CCAAT/enhancer binding protein β (C/EBP-β) transcription factors (Acosta et al., 2008; Chien et al., 2011). The paracrine effects of the SASP are thought to be protumorigenic and also contribute to age-related pathologies (Campisi, 2013; Muñoz-Espín and Serrano, 2014). Thus, it is ideal to maintain the senescence-associated cell cycle arrest while limiting the SASP to harness the benefits of senescence while limiting the detrimental aspect of the senescence program.

Another hallmark of cellular senescence is a robust alteration in the chromatin and epigenetic landscape (Chandra and Narita, 2013). In particular, chromatin in senescent cells is reorganized to form senescence-associated heterochromatin foci (SAHF), specialized heterochromatin that results from compaction of chromosomes (Narita et al., 2003; Zhang et al., 2007). Consistently, senescent cells display increased repressive histone marks such as H3K9me2/3 (Narita et al., 2003). SAHF and repressive epigenetic marks act in concert to decrease transcription of proliferation-promoting genes (Chandra et al., 2012). Indeed, proliferation-promoting gene loci are sequestered into SAHF (Narita et al., 2003; Zhang et al., 2007). In contrast, SASP gene transcription is robustly increased during senescence (Kuilman et al., 2008). How SASP genes are excluded from global SAHF-mediated gene silencing remains unclear.

High mobility group proteins are nonhistone chromatin-bound proteins that regulate gene transcription by altering chromatin architecture (Bianchi and Agresti, 2005). For example, the high mobility group box (HMGB) proteins such as

Correspondence to Rugang Zhang: rzhang@wistar.org

Abbreviations used: BAC, bacterial artificial chromosome; C/EBP-β, CCAAT/enhancer binding protein β; ChIP, chromatin immunoprecipitation; CRISPR, clustered regularly interspaced short palindromic repeat; gRNA, guide RNA; HMGB, high mobility group box; NF-κB, nuclear factor κB; qRT-PCR, quantitative RT-PCR; SA-β-Gal, senescence-associated β-galactosidase; SAHF, senescence-associated heterochromatin foci; SASP, senescence-associated secretory phenotype.

The Rockefeller University Press $30.00
J. Cell Biol. Vol. 215 No. 3 325–334
https://doi.org/10.1083/jcb.201608026

HMGB1 and HMGB2 bind to DNA without sequence specificity to increase the accessibility of the chromatin to transcription factors (Thomas, 2001). Thus, HMGB proteins are generally thought to promote transcription (Malarkey and Churchill, 2012). Although HMGB1 has previously been shown to redistribute from nuclei to the extracellular milieu during senescence as a secreted alarmin (Davalos et al., 2013), the role of HMGB2 during senescence is unclear. Here, we determined that HMGB2 orchestrates the SASP through prevention of heterochromatin spreading to allow for the exclusion of SASP gene loci from SAHF-mediated gene silencing.

Results and discussion

HMGB2 expression is regulated during senescence

Senescent cells display marked changes in chromatin, which directly affects transcription of many genes (Narita et al., 2003; Zhang et al., 2007). We therefore wanted to identify factors in senescent cells that are directly involved in regulating the chromatin landscape. We cross-referenced four publically available gene expression datasets (Narita et al., 2009; Aksoy et al., 2012; Nelson et al., 2014; Takebayashi et al., 2015) to identify genes encoding chromatin regulatory proteins (Nelson et al., 2014) that are significantly altered in senescent cells across all four datasets (Fig. 1 A). From this analysis, only seven genes were identified (Table S3). The top hit in all four datasets was HMGB2 (Fig. 1 A). Indeed, we validated that HMGB2 expression was decreased at both the mRNA and protein levels during senescence of normal primary human embryonic fibroblast IMR90 cells induced by oncogenic RAS (Fig. 1, B and C; and Fig. S1, A–C). Similar to a previous study (Biniossek et al., 2013), *HMGB2* was also down-regulated in senescent IMR90 cells induced by extended passaging compared with young cells (Figs. 1 D and S1, D and E). Similar observations were made using senescent cells isolated from the accelerated aging G4 *mTerc*$^{-/-}$ mouse model (Rudolph et al., 1999) compared with wild-type controls (Figs. 1 E and S1, F–H). Consistently, knockdown or knockout of HMGB2 induced senescence in IMR90 cells (Fig. S1, I–O). Interestingly, senescence induced by HMGB2 inhibition had little effect on SASP gene expression (Fig. S1 P). Notably, although HMGB2 is markedly decreased at both the mRNA and in the total cell lysate protein level, a significant proportion remained bound to chromatin isolated from senescent cells (Fig. 1 F). The homologous HMGB1 was decreased at the protein level (Fig. 1 F), which is consistent with previous studies of redistribution of HMGB1 from nuclei to the extracellular milieu during senescence (Davalos et al., 2013; Wiley et al., 2016). HMGB2 regulates gene transcription by changing chromatin architecture (Thomas, 2001). This suggests that HMGB2 might play a role in chromatin architecture to modulate gene expression during senescence.

HMGB2 preferentially binds to SASP gene loci in senescent cells

To understand the potential role of HMGB2 in senescence, we performed chromatin immunoprecipitation (ChIP) followed by next-generation sequencing (ChIP-Seq) to determine the localization of HMGB2 in senescent cells (GEO accession no. GSE85057). Because HMGB2 typically promotes gene transcription (Thomas, 2001; Bianchi and Agresti, 2005; Malarkey and Churchill, 2012), we cross-referenced HMGB2 ChIP-Seq data with gene expression profiles (Aksoy et al., 2012; Takebayashi et al., 2015) and focused on the genes with increased HMGB2 association that are up-regulated during senescence. This analysis revealed 89 genes that are both significantly up-regulated and displayed significant HMGB2 enrichment during senescence ($P = 0.0027$ vs. binding to a random set of genes; Fig. 2 A). Pathway analysis revealed that the main clusters of functions regulated by the identified HMGB2 regulated genes included cytokines, chemokines, secreted factors, and metalloproteinases (Fig. 2 A and Table S4). Many of these genes (Fig. 2 B) are known SASP factors, which contribute to the detrimental effects of senescence on tumor promotion and aging (Coppé et al., 2010; Pérez-Mancera et al., 2014; van Deursen, 2014). Strikingly, statistical analysis revealed that HMGB2 enrichment on SASP genes was 24.5-fold more than on a random set of genes ($P < 10^{-12}$). HMGB2 was enriched at many SASP gene loci (for example, *IL1β*, *IL8*, and *IL6*; Fig. 2 C). These findings suggest that HMGB2's association may allow for expression of SASP genes. These results were independently validated by ChIP analysis using an anti-HMGB2 antibody in control and oncogenic RAS-induced senescent IMR90 cells (Fig. 2, D and E).

To determine whether HMGB2 is localized on SASP gene loci in other forms of senescence, we used mouse senescent ear fibroblast cells from the premature aging G4 *mTerc*$^{-/-}$ mouse model (Fig. S1, F–H). These cells also showed increased SASP gene expression, which correlated with an increased association of HMGB2 to these loci in ChIP experiments (Fig. 2, F and G). As a control, HMGB1, which shows sequence homology to HMGB2, did not bind to SASP gene loci during senescence (Fig. S2 A). This is consistent with a previous study showing that HMGB1 is mostly redistributed from nuclei to the extracellular milieu as a secreted alarmin (Davalos et al., 2013). HMGB2 is known to regulate gene transcription, and NF-κB and C/EBP-β are known transcription factors that regulate SASP (Acosta et al., 2008; Chien et al., 2011). Thus, we determined whether HMGB2's association with SASP gene loci is regulated by NF-κB and/or C/EBP-β. Notably, HMGB2 binding to SASP gene loci was independent of NF-κB because knockdown of the p65 subunit of NF-κB did not alter HMGB2 binding to SASP gene loci (Fig. S2, B–E). In addition, C/EBP-β is a direct target gene of HMGB2 in senescent cells (Fig. 2, A and B; and Fig. S2 F), and knockdown of HMGB2 decreased *C/EBP-β* gene expression (Fig. S2, G and H). Collectively, these data suggest that HMGB2 is a novel regulator of the SASP.

Loss of HMGB2 blunts SASP gene expression

Because HMGB2 localizes to SASP gene loci during senescence (Fig. 2), we next determined whether HMGB2 is required for SASP gene expression. We knocked down HMGB2 using an shRNA in senescent cells (Fig. 3 A). Knockdown of HMGB2 significantly decreased HMGB2 protein levels in both total cell lysates and chromatin fractions (Fig. 3 B). The decrease in chromatin-bound HMGB2 in senescent cells correlated with a decrease in SASP gene expression (Figs. 3 C and S3, A and B). Similar results were also obtained using a heterogeneous population of HMGB2 CRISPR (clustered regularly interspaced short palindromic repeat) knockout cells (Fig. 3, D and E; and Fig. S3 C). Note that loss of

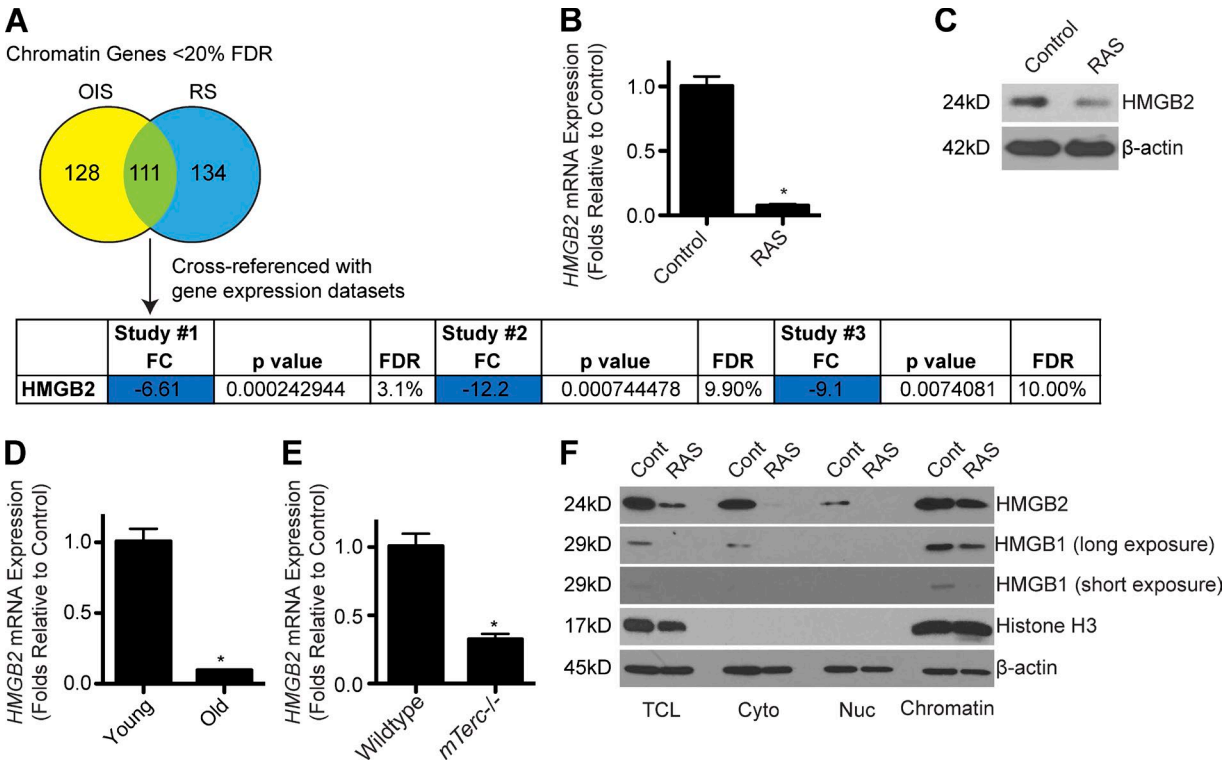

	Study #1 FC	p value	FDR	Study #2 FC	p value	FDR	Study #3 FC	p value	FDR
HMGB2	-6.61	0.000242944	3.1%	-12.2	0.000744478	9.90%	-9.1	0.0074081	10.00%

Figure 1. **HMGB2 expression is altered during senescence.** (A) Using publically available microarray databases, the most significantly altered chromatin-related genes during senescence were identified. Only genes that were significantly ($P < 0.05$) altered more than twofold in all four datasets were considered "hits." Study #1: GEO accession no. GSE28464; study #2: GEO accession no. GSE40349; and study #3: GEO accession no. GSE60652. FC, fold change; FDR, false discovery rate; OIS, oncogene-induced senescence; RS, replicative senescence. (B) IMR90 cells were infected with retrovirus encoding oncogenic RAS to induce senescence or control. Cells were selected for 3 d with 1 µg/ml puromycin. 4 d later, *HMGB2* mRNA expression was determined. (C) Same as B, but HMGB2 protein expression was determined in total protein lysates by immunoblot. β-Actin was used as a loading control. (D) *HMGB2* mRNA expression was determined in young (PD24) and old senescent (PD60) IMR90 fibroblasts. (E) *HMGB2* mRNA expression was determined in senescent G4 *mTerc*$^{-/-}$ or wild-type control ear fibroblasts. (B, D, and E) *B2M* expression was used as an internal control. (F) Same as B, but total cell lysates (TCL), cytoplasmic fraction (Cyto), nuclear soluble fraction (Nuc), and chromatin-bound fraction (Chromatin) were isolated, and HMGB2 and HMGB1 protein expression was determined. Long and short film exposures are shown for HMGB1. Histone H3 and β-actin were used as loading controls. For all panels, graphs shown are the mean and SEM of triplicates from a representative experiment that was independently repeated at least three times. *, $P < 0.05$ versus control.

HMGB2 induces senescence, and IMR90s are primary cells that will senesce as a result of extended passage, which together prevented us from obtaining single HMGB2 CRISPR clones. Interestingly, loss of chromatin-bound HMGB2 and SASP gene expression did not alter the senescence status of these cells, as demonstrated by the senescence marker senescence-associated β-galactosidase (SA-β-Gal) staining and senescence-associated cell cycle arrest assayed by colony formation (Fig. 3, F–I; and Fig. S3, D–G). This was not caused by a loss of the senescence inducer, as RAS was expressed at comparable levels in both shHMGB2/RAS and RAS-alone controls (Fig. S3, C and H). Although the cell cycle arrest phenotype of senescence is tumor suppressive, the detrimental side effects of the SASP have tumor-promoting characteristics and may also play a role in tissue aging (Pérez-Mancera et al., 2014; van Deursen, 2014). Previous approaches to inhibit the SASP often compromise the tumor-suppressive senescence-associated cell cycle arrest. For example, inhibition of other regulators of the SASP, such as NF-κB, does not maintain the cell cycle arrest (Chien et al., 2011). This suggests that inhibition of HMGB2 represents a unique strategy to uncouple the senescence-associated cell cycle arrest from the SASP to allow for limiting SASP while maintaining the cell cycle arrest.

Loss of HMGB2 allows for senescence-associated heterochromatin spreading into SASP gene loci and promotes the inclusion of SASP gene loci into SAHF

SASP genes are highly expressed during senescence (Coppé et al., 2010). Consistently, these genes display decreased repressive histone marks, such as H3K9me2/3, that are found in SAHF and contribute to silencing of proliferation-promoting genes (Figs. 4 A and S3, I and J; Narita et al., 2003; Zhang et al., 2007). Consistent with HMGB2's selective localization to SASP gene loci and the fact that HMGB2 loss does not affect the senescence-associated cell cycle arrest (Fig. 3, F–I), loss of HMGB2 did not affect SAHF formation (Fig. 4, B and C; and Fig. S3 K). We therefore hypothesized that HMGB2's association with SASP gene loci allows for the exclusion of SASP gene loci from SAHF-mediated gene silencing. Consequently, loss of HMGB2, which decreases SASP gene expression (Fig. 3), may allow for localized spreading of heterochromatin to repress SASP gene transcription. To test this hypothesis, we determined whether HMGB2 loss promotes the incorporation of SASP gene loci into SAHF. To do so, we first performed 3D DNA-FISH experiments using a bacterial artificial chromosome (BAC) containing the human *IL8* gene locus. Indeed, the results showed that this locus is

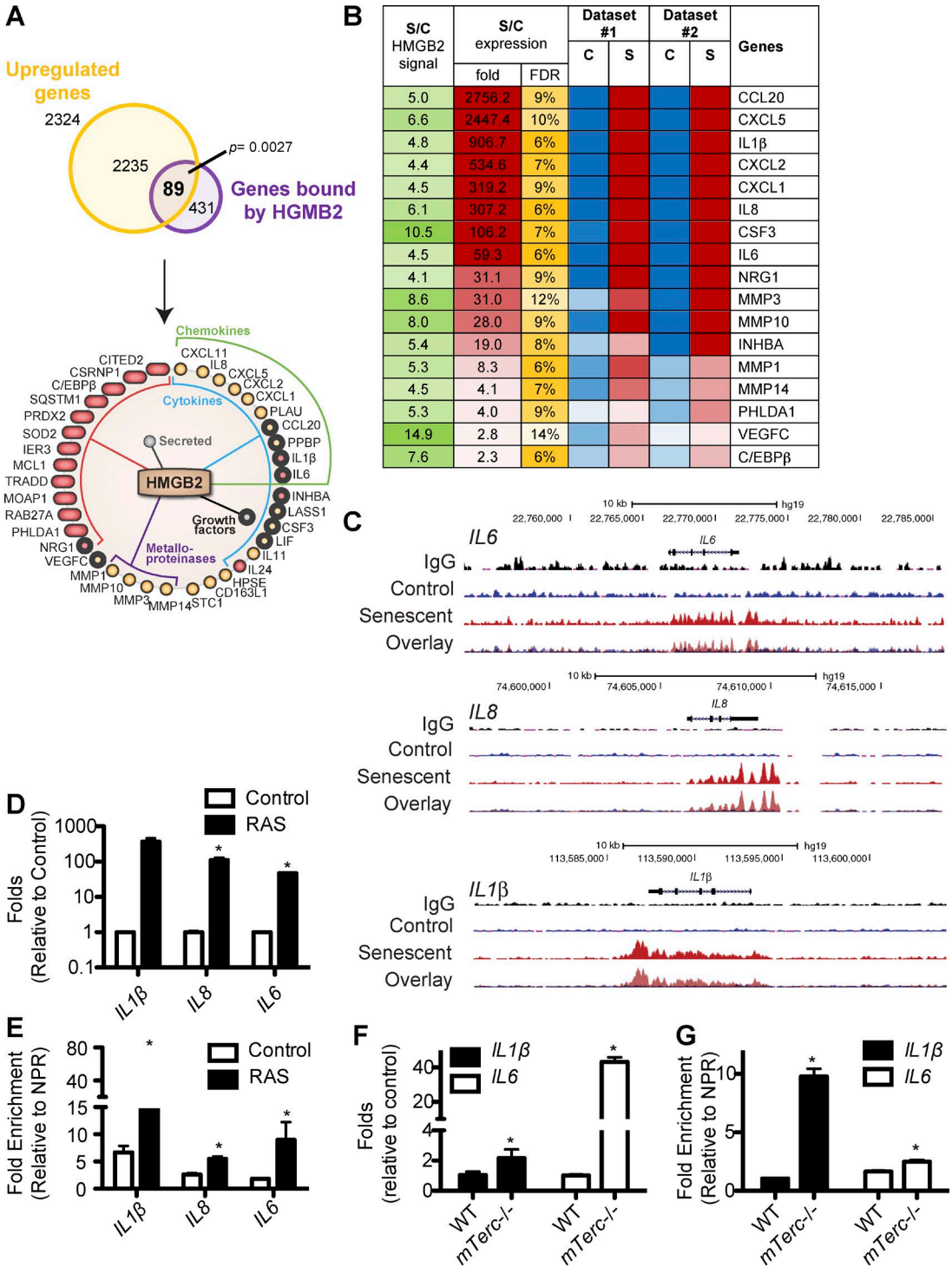

S/C HMGB2 signal	S/C expression		Dataset #1		Dataset #2		Genes
	fold	FDR	C	S	C	S	
5.0	2756.2	9%					CCL20
6.6	2447.4	10%					CXCL5
4.8	906.7	6%					IL1β
4.4	534.6	7%					CXCL2
4.5	319.2	9%					CXCL1
6.1	307.2	6%					IL8
10.5	106.2	7%					CSF3
4.5	59.3	6%					IL6
4.1	31.1	9%					NRG1
8.6	31.0	12%					MMP3
8.0	28.0	9%					MMP10
5.4	19.0	8%					INHBA
5.3	8.3	6%					MMP1
4.5	4.1	7%					MMP14
5.3	4.0	9%					PHLDA1
14.9	2.8	14%					VEGFC
7.6	2.3	6%					C/EBPβ

Figure 2. **HMGB2 preferentially binds to SASP gene loci in senescent cells.** (A) HMGB2 ChIP-Seq data (GEO accession no. GSE85057) were cross-referenced with publically available microarray datasets. 89 genes were bound by HMGB2 and had increased expression in senescent cells. The significance of gene overlap was estimated and showed a significant enrichment in HMGB2-bound up-regulated genes compared with a random set of genes (P = 0.0027). The identified genes were subjected to pathway enrichment analysis by DAVID software. (B) Heatmap of SASP genes preferentially bound by HMGB2 during senescence. The ratio of HMGB2 ChIP signal and expression of the indicated genes in senescent (S) and control (C) is listed in dataset #1 (GEO accession no. GSE40349) and dataset #2 (GEO accession no. GSE60652). Green represents the signal intensity in the HMGB2 ChIP-Seq in senescent cells versus control. Red represents up-regulated genes, whereas blue represents down-regulated genes. Yellow represents the false discovery rate (FDR). (C) Representative tracks from HMGB2 ChIP-Seq for *IL1β*, *IL8*, and *IL6*. (D) IMR90 cells were infected with retrovirus encoding oncogenic RAS to induce senescence or controls. Cells were selected for 3 d with 1 µg/ml puromycin. 4 d later, *IL1β*, *IL8*, and *IL6* mRNA expression was determined. *B2M* was used as an internal control. (E) Same as D, but HMGB2 ChIP was performed, and HMGB2 binding to *IL1β*, *IL8*, and *IL6* was determined by quantitative PCR and normalized to a nonpeak region control. (F) Expression of *IL1β* and *IL6* mRNA was determined by qRT-PCR in senescent G4 *mTerc*$^{-/-}$ and wild-type (WT) control mouse ear fibroblasts. *B2M* expression was used as an internal control. (G) Same as F, but HMGB2 ChIP was performed. HMGB2 binding to *IL1β* and *IL6* was determined by quantitative PCR and normalized to a nonpeak region (NPR) control. For all panels, graphs shown are the mean and SEM of triplicates from a representative experiment that was independently repeated at least three times. *, P < 0.05 versus control.

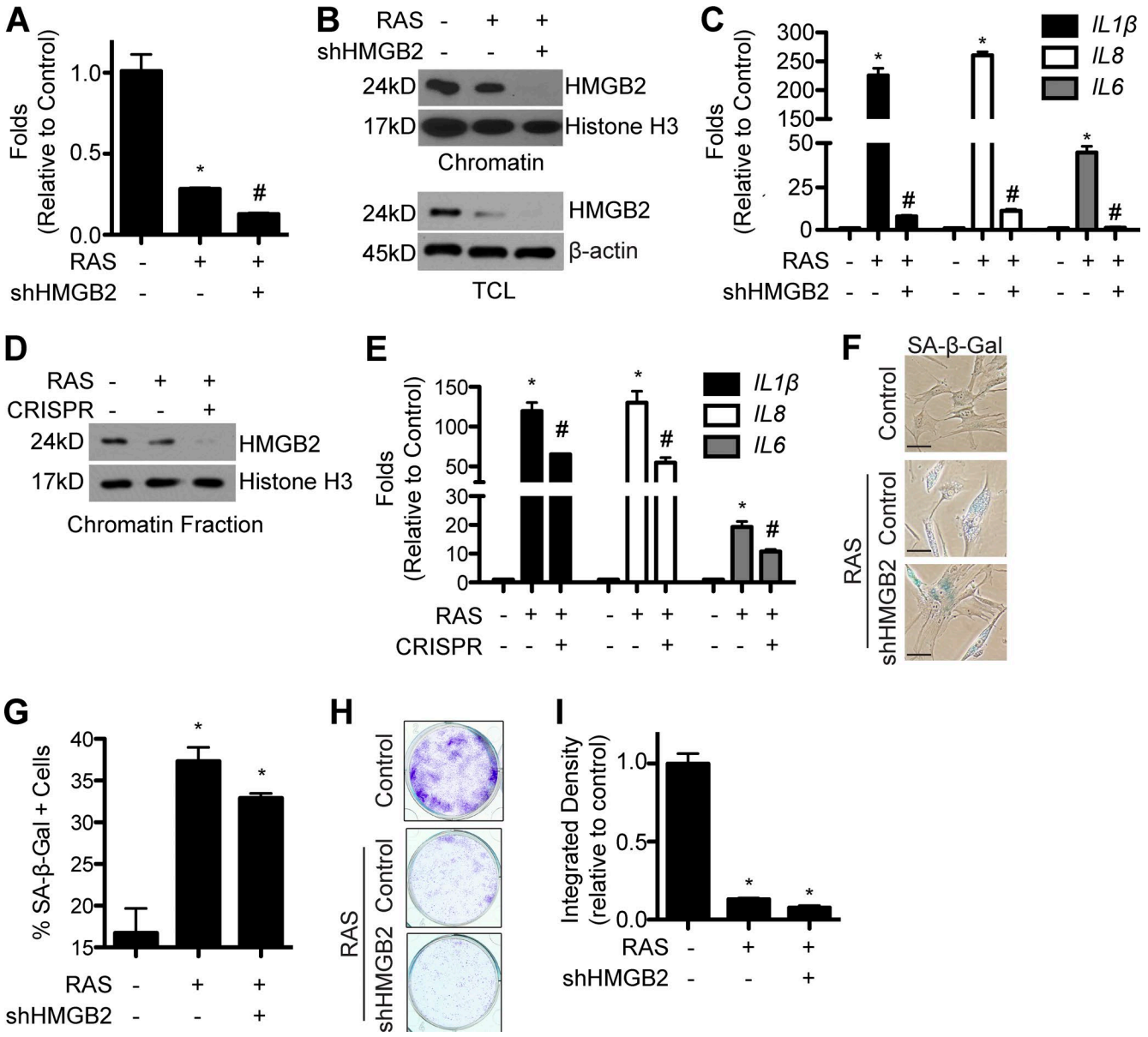

Figure 3. **Loss of HMGB2 blunts SASP gene expression while maintaining the senescence-associated cell growth arrest.** (A) IMR90 cells were infected with retrovirus encoding oncogenic RAS alone or in combination with a lentivirus expressing an shRNA to the human *HMGB2* gene (shHMGB2). Cells were selected for 3 d with 3 µg/ml puromycin. 4 d later, *HMGB2* mRNA expression was determined. (B) Same as A, but both total cell lysates (TCL) and chromatin fractions were isolated, and HMGB2 protein expression was determined. Histone H3 and β-actin were used as internal loading controls. (C) Same as A, but *IL1β*, *IL8*, and *IL6* mRNA expression was determined. (D) IMR90 cells were infected with retrovirus encoding oncogenic RAS alone or in combination with a Cas9-expressing lentivirus expressing a gRNA to HMGB2 (CRISPR). Cells were selected for 3 d with 3 µg/ml puromycin. 4 d later, the chromatin fraction was isolated, and HMGB2 protein expression was determined. Histone H3 was used as an internal loading control. (E) Same as D, but *IL1β*, *IL8*, and *IL6* mRNA expression was determined. (A, C, and E) *B2M* was used as an internal control. (F) Same as A, but SA-β-Gal staining was performed. Bars, 5 µm. (G) Quantification of F. (H) Same as A, but an equal number of cells were seeded into 6-well plates and stained with crystal violet 14 d later. (I) Quantification of H. Graphs shown are the mean and SEM of triplicates from a representative experiment that was independently repeated at least three times. *, $P < 0.05$ versus control; #, $P < 0.05$ versus RAS.

mostly excluded from SAHF in senescent cells (Fig. 4, D and E; and Fig. S3 L). In contrast, the proliferation-promoting *CCNA2* gene locus is sequestered into SAHF (Narita et al., 2003; Zhang et al., 2007). We next directly determined the effects of HMGB2 loss on the localization of SASP gene loci relative to SAHF in senescent cells. Toward this goal, we measured the distance between the FISH signal and the closest SAHF foci. Indeed, knockdown of HMGB2 promoted the inclusion of the *IL8* gene locus into SAHF in senescent cells (Fig. 4, D and E; and Fig. S3 M).

We next directly determined whether loss of HMGB2 allows for the spreading of heterochromatin marks into the SASP gene loci. To do so, we performed ChIP analysis of H3K9me2, a repressive epigenetic mark known to be part of SAHF (Narita et al., 2003; Zhang et al., 2007). Indeed, the repressive H3K9me2 epigenetic mark was decreased at SASP gene loci in senescent cells, which corresponded to HMGB2 enrichment (Figs. 4 F and S3 N). Excitingly, knockdown of HMGB2 in senescent cells increased H3K9me2's enrichment at SASP gene loci compared with controls (Figs. 4 F and S3 N). Similar

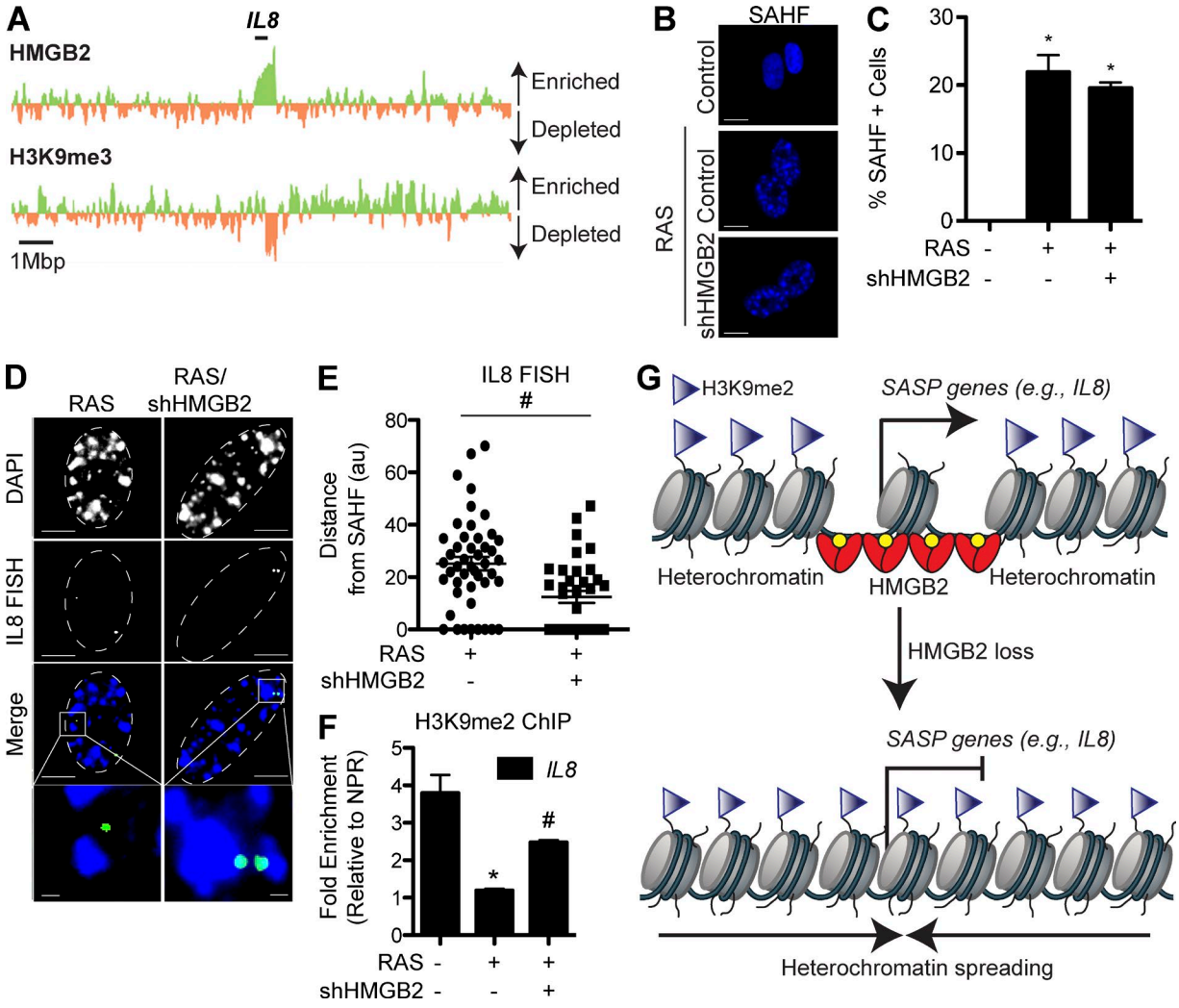

Figure 4. **Loss of HMGB2 allows for spreading of heterochromatin and promotes the inclusion of SASP gene loci in SAHF.** (A) Cross-referencing of HMGB2 ChIP-Seq data and H3K9me3 ChIP-Seq data at the *IL8* locus. Green indicates enrichment of HMGB2 or H3K9me3 binding in senescent cells, whereas orange indicates depletion of HMGB2 or H3K9me3 binding in senescent cells. The black bar indicates the *IL8* genomic locus. (B) IMR90 cells were infected with retrovirus encoding oncogenic RAS alone or in combination with a lentivirus expressing an shRNA to HMGB2. Cells were selected for 3 d with 3 µg/ml puromycin. 4 d later, cells were stained for SAHF using DAPI. Bars, 10 µm. (C) Quantification of B. (D) Same as B, but 3D DNA-FISH was performed with a BAC containing the *IL8* gene locus. White dashed lines indicate the nucleus. Bars: (top) 5 µm; (inset) 0.5 µm. (E) Quantification of 3D DNA-FISH. The distance between *IL8* loci and the nearest SAHF was determined using ImageJ software (au, arbitrary units). At least 50 nuclei were quantified. Horizontal bars denote the comparison between RAS alone and RAS/shHMGB2. (F) Same as B, but H3K9me2 ChIP was performed, and H3K9me2 binding to *IL8* was determined by quantitative PCR and normalized to a nonpeak region (NPR) control. (G) Scheme of how HMGB2 binds to SASP genes to promote their transcription (left). Loss of HMGB2 allows for spreading of repressive senescence-associated heterochromatin to inhibit SASP gene expression (right). Graphs shown are the mean and SEM of triplicates from a representative experiment that was independently repeated at least three times. *, $P < 0.05$ versus control; #, $P < 0.05$ versus RAS.

results were observed in the heterogeneous HMGB2 CRISPR knockout population (Fig. S3 O). These results support the notion that HMGB2's association with SASP gene loci prevents the spreading of heterochromatin marks into SASP gene loci.

Collectively, these data support a model whereby chromatin-bound HMGB2 promotes SASP gene expression through preventing the spreading of heterochromatin marks and allows for the exclusion of SASP gene loci from SAHF-mediated global gene silencing (Fig. 4 G). Consequently, loss of HMGB2 allows for spreading of heterochromatin marks and promotes the inclusion of SASP gene loci into SAHF, which in turn represses SASP gene expression (Fig. 4 G). These data suggest that inhibition of HMGB2 will uncouple the detrimental SASP from the beneficial tumor-suppressive senescence-associated cell cycle arrest. This study represents the first in its class approach that incorporates SASP gene loci into SAHF to silence their expression while maintaining SAHF-mediated gene silencing of proliferation-promoting genes.

Materials and methods

Cells and culture conditions

Normal diploid IMR90 human fibroblasts were cultured according to the ATCC in low oxygen (2%) in DMEM (4.5 g/l glucose) with 10% FBS supplemented with L-glutamine, nonessential amino acids, sodium pyruvate, and sodium bicarbonate. Experiments were performed on IMR90 between population doublings #25 and 35 except where

otherwise indicated. Wild-type and G4 *mTerc*$^{-/-}$ ear fibroblasts were obtained from C57BL6/J background mice and cultured as described previously (Du et al., 2004), except using a 2% oxygen concentration, in DMEM (4.5 g/l glucose, no sodium pyruvate) with 15% FBS.

Plasmids and antibodies

pBABE-puro-H-RAS^{G12V} and pLentiCRISPR v2 were obtained from Addgene. pLentiCRISPR-HMGB2 was constructed by inserting the HMGB2 guide RNA (gRNA; 5′-AACACCCTGGCCTATCCATT-3′) according to previously published methods (Sanjana et al., 2014). In brief, pLentiCRISPR v2 was digested and dephosphorylated with BsmBI restriction enzyme for 30 min at 37°C. The digested plasmid was run on a 1% agarose gel, cut out, and purified using the Wizard SV Gel and PCR Clean Up kit (Promega). The oligonucleotides were phosphorylated using T4 PNK (M0201S) with T4 Ligation Buffer (New England Biolabs, Inc.). Samples were annealed in a thermocycler at 37°C for 30 min and then at 95°C for 5 min and then were ramped down to 25°C at 5°C/min. Annealed oligonucleotides were diluted 1:200 in RNase/DNase-free water. Ligation of the annealed oligonucleotide and digested pLentiCRISPR v2 plasmid was performed using Quick Ligase (New England Biolabs, Inc.). pLKO.1-shHMGB2 (shHMGB2 #1: TRCN000000150009; shHMGB #2: TRCN0000019011) and pLKO.1-shNF-κB (p65 subunit; TRCN0000014687) plasmids were obtained from The Wistar Institute Molecular Screening Facility.

The following antibodies were obtained from the indicated suppliers: rabbit anti-HMGB2 (Abcam), rabbit anti-HMGB1 (Abcam), rabbit antihistone H3 (EMD Millipore), mouse anti–β-actin (Sigma-Aldrich), mouse anti-RAS (BD), rabbit anti-pS10H3 (Santa Cruz Biotechnology, Inc.), and mouse anti–cyclin A (Leica Biosystems).

Retrovirus and lentivirus infection

Retrovirus production and transduction were performed as described previously using the BES-buffered saline/calcium chloride method (Aird et al., 2013). Phoenix cells were used to package the infection viruses (a gift from G. Nolan, Stanford University, Palo Alto, CA). Lentivirus was packaged using the ViraPower kit (Invitrogen) as per the manufacturer's instructions and as described previously (Ye et al., 2007; Li et al., 2010; Tu et al., 2011). Cells infected with viruses encoding the puromycin resistance gene were selected in 1 µg/ml puromycin unless otherwise indicated.

Immunoblotting

Cells were lysed in 1× sample buffer (2% SDS, 10% glycerol, 0.01% bromophenol blue, 62.5 mM Tris, pH 6.8, and 0.1 M DTT) and heated to 95°C for 10 min. Protein concentrations were determined using the Bradford assay. An equal amount of total protein was resolved using SDS-PAGE gels and transferred to nitrocellulose membranes at 100 mA for 2 h at 4°C. Membranes were blocked with 5% nonfat milk in TBS containing 0.1% Tween 20 (TBS-T) for 1 h at room temperature. Membranes were incubated overnight at 4°C in the primary antibodies indicated in the Plasmids and antibodies section in 4% BSA/TBS + 0.025% sodium azide. Membranes were washed four times in TBS-T for 5 min at room temperature, after which they were incubated with HRP-conjugated secondary antibodies (Cell Signaling Technology) for 1 h at room temperature. After washing four times in TBS-T for 5 min at room temperature, proteins were visualized on film after incubation with SuperSignal West Pico PLUS Chemiluminescent Substrate (Thermo Fisher Scientific).

Chromatin fractionation was performed as described previously (Tu et al., 2011). In brief, cells were trypsinized and pelleted by centrifugation at 1,000 rpm, after which they were washed once in PBS. The pellets were then resuspended in 300 µl buffer A (10 mM Hepes-KOH, pH 8.0, 10 mM KCl, 1.5 mM $MgCl_2$, 0.34 M sucrose, and 10% glycerol, pH 7.5, plus the EDTA-free Protease Inhibitor Cocktail [Roche], 1 mM DTT, and 0.1 mM PMSF) with 0.1% Triton X-100. Cells were incubated on ice for 5 min and then pelleted at 1,300 *g* for 4 min at 4°C. The supernatant was kept as the cytoplasmic fraction. The pellet was washed once in buffer A, after which it was resuspended in 300 µl buffer B (3 mM EDTA, pH 8.0, and 0.2 mM EGTA, pH 8.0, plus the EDTA-free Protease Inhibitor Cocktail, 1 mM DTT, and 0.1 mM PMSF). Samples were incubated on ice for 30 min and then centrifuged at 1,700 *g* for 4 min at 4°C. The supernatant was kept as the nucleoplasmic fraction. The pellet was washed once in buffer B and finally resuspended in 1× sample buffer.

DAPI and SA-β-Gal staining

DAPI staining was performed as described previously (Zhang et al., 2007). Cells were fixed for 10 min using 4% paraformaldehyde and then solubilized for 5 min with 0.2% Triton X-100 in PBS. Cells were incubated with 0.15 µg/ml DAPI for 1 min to stain for SAHF. Coverslips were mounted in mounting media (1 µg/ml *p*-phenylenediamine, pH 9.0, in 90% glycerol) and sealed with nail polish. Cells were visualized at room temperature using an Eclipse T*i* microscope (Nikon) with a CFI Plan Fluor 40×/0.75-NA objective. Images were acquired using a DS-Qi1 camera (Nikon) with NIS Elements software (Nikon) and processed using ImageJ software (National Institutes of Health).

SA-β-Gal staining was performed as previously described (Dimri et al., 1995). Cells were fixed for 5 min at room temperature in 2% formaldehyde/0.2 glutaraldehyde in PBS. After washing the cells twice with PBS, cells were stained at 37°C overnight in a non-CO_2 incubator in staining solution (40 mM Na_2HPO_4, pH 6.0, 150 mM NaCl, 2 mM $MgCl_2$, 5 mM $K_3Fe(CN)_6$, 5 mM $K_4Fe(CN)_6$, and 1 mg/ml X-gal). Images were acquired at room temperature using an Eclipse TS-100 inverted microscope (Nikon) with a 20×/0.4-NA objective equipped with a DS-Fi1 camera (Nikon).

Colony formation assay

For colony formation, an equal number of cells (1,000 cells/well) was inoculated in 6-well plates and cultured for an additional 2 wk. Colony formation was visualized by fixing the plates for 5 min with 1% paraformaldehyde, after which they were stained with 0.05% crystal violet as previously described (Tu et al., 2011). Integrated density was determined using ImageJ software.

Quantitative RT-PCR (qRT-PCR)

RNA was extracted from cells using TRIzol (Thermo Fisher Scientific) and DNase treated using RNeasy columns (QIAGEN). Expression of mRNA levels for *IL6*, *IL8*, *IL1β*, and *HMGB2* (Taqman primers from Invitrogen) was determined using Platinum Quantitative RT-PCR ThermoScript One-Step System (Invitrogen) master mix on a Chromo4 machine (Bio-Rad Laboratories). *β-2-microglobulin* (*B2M*; Taqman) was used as an internal control. Expression of all other RNAs was determined using iTaq Universal SYBR Green Supermix (Bio-Rad Laboratories) master mix. *B2M* was used as an internal control. Primer sequences can be found in Table S1. All qRT-PCR data were normalized to *B2M*, and fold change was calculated using the ΔΔC(t) method.

ChIP and ChIP-Seq analysis

ChIP was performed using ChIP-grade antibodies: rabbit anti-HMGB2 and mouse anti-H3K9me2. Cells were fixed in 1% paraformaldehyde for 5 min at room temperature and then quenched with 1 ml of 2.5 M glycine for 5 min at room temperature. Cells were washed twice with cold PBS. Cells were lysed in 1 ml ChIP lysis buffer (50 mM Hepes-KOH, pH 7.5, 140 mM NaCl, 1 mM EDTA, pH 8.0, 1% Triton X-100,

and 0.1% deoxycholate [DOC] with 0.1 mM PMSF and the EDTA-free Protease Inhibitor Cocktail). Samples were incubated on ice for 10 min and then centrifuged at 3,000 rpm for 3 min at 4°C. The pellet was resuspended in 500 µl lysis buffer 2 (10 mM Tris, pH 8.0, 200 mM NaCl, 1 mM EDTA, and 0.5 mM EGTA with 0.1 mM PMSF and the EDTA-free Protease Inhibitor Cocktail) and incubated at room temperature for 10 min. Samples were centrifuged at 3,000 rpm for 5 min at 4°C. Next, the pellet was resuspended in 300 µl lysis buffer 3 (10 mM Tris, pH 8.0, 100 mM NaCl, 1 mM EDTA, 0.5 mM EGTA, 0.1% DOC, and 0.5% *N*-lauroylsarcosine with 0.1 mM PMSF and the EDTA-free Protease Inhibitor Cocktail). Cells were sonicated using a Biorupter (Diagenode) for 15 min (30 s on, 1 min off). Next, 30 µl of 10% Triton X-100 was added to each tube, and then samples were centrifuged at max speed for 15 min at 4°C. The supernatant was transferred to new tubes, and the DNA concentration was quantified. Samples were precleared for 1 h at 4°C on a rotator using 15 µl protein G Dynabeads (Thermo Fisher Scientific) in ChIP lysis buffer. Samples were centrifuged at max speed for 15 min at 4°C, after which the supernatant was transferred to a new tube. 50 µl of the antibody bead conjugate solution was added, and chromatin was immunoprecipitated overnight on a rotator at 4°C. The following washes were performed for 15 min each by rotating for 15 min at 4°C: ChIP lysis buffer (twice), ChIP lysis buffer + 0.65 M NaCl, wash buffer (10 mM Tris-HCl, pH 8.0, 250 mM LiCl, 0.5% NP-30, 0.5% DOC, and 1 mM EDTA, pH 8.0), and TE (10 mM Tris-HCl, pH 8.0, and 1 mM EDTA, pH 8.0). DNA was eluted by incubating the beads with TES (50 mM Tris-HCl, pH 8.0, 10 mM EDTA, pH 8.0, and 1% SDS) for 30 min at 65°C. Reversal of cross-linking was performed by incubating samples overnight at 65°C. Proteins were digested using 1 mg/ml proteinase K and incubating at 37°C for 5 h. Finally, the DNA was purified using the Wizard SV Gel and PCR Clean Up kit (Promega).

Immunoprecipitated DNA was analyzed using KiCqstart SYBR Green Readymix (Sigma-Aldrich). Enrichment of HMGB2 or H3K9me2 was determined by normalizing to a nonpeak region control. Primer sequences can be found in Table S2.

For next-generation sequencing, ChIP-Seq libraries were prepared from 10 ng ChIP DNAs with the NEBNext Ultra DNA Library Prep kit for Illumina (New England Biolabs, Inc.) according to the manufacturer's protocol. The ChIP-Seq libraries were amplified with 12 cycles by using Q5 high-fidelity DNA polymerase (New England Biolabs, Inc.) and sequenced in a 75-bp single end run using a Next Seq 500 (Illumina).

3D DNA-FISH

The BAC clone RP11-997L11 containing the *IL8* gene loci was purchased from the Children's Hospital Oakland Research Institute. 3D DNA-FISH was performed as described previously (Zhang et al., 2007). Probes were labeled using the BioPrimer DNA Labeling System kit (Invitrogen). Labeled BAC probes were prepared for use by combining a 300-ng-labeled BAC probe, 22 µg Cot1 DNA (Invitrogen), 5.5 µl of 3 M NaAc, and 150 µl of 100% EtOH. The solution was gently mixed and incubated at −80°C for 1 h. Samples were centrifuged at max speed for 20 min at 4°C, washed once with 70% EtOH, and dried. Pellets were resuspended in 50% formamide/2× SSC/10% dextran sulfate and dissolved at 37°C for 20 min. Probes were denatured for 5 min at 73°C and then preannealed for 30 min at 37°C.

For FISH, cells were seeded onto coverslips in 6-well plates and allowed to attach overnight. Coverslips were washed twice with PBS and then incubated in 3 ml of 0.075 M KCl for 20 min at room temperature (hypotonic treatment). 0.5 ml of fresh fixative (3:1 MeOH/acetic acid) was added to the KCl, and samples were incubated for 10 min at room temperature. The solution was removed, and cells were fixed in 3:1 MeOH/acetic acid overnight at 20°C. Coverslips were washed three times with 2 ml of fresh fixative, after which coverslips were steam dried for 1 min. Cells were treated with 100 µg/ml RNase A/2× SSC for 1 h at 37°C, after which they were washed four times for 2 min each in 2× SSC. Cells were treated with 0.1 mg/ml pepsin/0.01 M HCl for 3 min at 37°C, after which they were washed once with PBS. Cells were postfixed in 1% paraformaldehyde containing 50 mM $MgCl_2$ for 10 min at room temperature and then washed once with PBS. Next, cells were dehydrated in an EtOH series (at 70%, 80%, and then 100% concentrations) for 2 min each and dried. DNA was denatured in 70% formamide/2× SSC at 73°C for 3 min, and then coverslips were immediately dehydrated as described in the previous sentence and dried. Cells were hybridized to the probe overnight at 37°C. Coverslips were washed for 10 min at 43°C with prewarmed 50% formamide/2× SSC (twice), for 4 min at 37°C with prewarmed 2× SSC (twice), and for 5 min at room temperature with 1× PBS (4× SSC, pH 7.0, and 0.05% Tween 20). To detect the biotinylated probe, coverslips were first blocked with 4× SSC/0.05% Tween 20/5% milk for 30 min at room temperature. Coverslips were incubated with FITC–Avidin D cell sorting grade (1:200; Vector Laboratories) for 30 min at room temperature and then washed for 5 min at room temperature in 4× SSC/0.05% Tween 20/5% milk while shaking. Next, coverslips were incubated with biotinylated anti–Avidin D9 (1:50; Vector Laboratories) for 30 min at room temperature and then washed for 5 min at room temperature in 4× SSC/0.05% Tween 20/5% milk while shaking. Finally, coverslips were incubated with FITC–Avidin D cell sorting (1:200; Vector Laboratories) for 30 min at room temperature and then washed for 5 min at room temperature in 4× SSC/0.05% Tween 20/5% milk while shaking. DAPI was used to stain for nuclei and SAHF as described in the DAPI and SA-β-Gal staining section. Coverslips were mounted in mounting media (1 µg/ml *p*-phenylenediamine, pH 9.0, in 90% glycerol) and sealed using nail polish. Cells were visualized at room temperature using an Eclipse T*i* microscope with a 100×/1.40-NA oil objective. Images were acquired using a DS-Qi1 camera with NIS Elements software and processed using ImageJ software.

Bioinformatics and statistical analysis

ChIP-Seq files are available in the GEO database (accession no. GSE85057). For ChIP-Seq, alignment was done versus the hg19 version of the human genome using the Bowtie algorithm (Langmead et al., 2009). We identified 364 HMGB2 broad peaks in senescent cells using the HOMER algorithm (Heinz et al., 2010) with the "-histone" option. Two gene expression datasets that test global transcriptome differences between control and RAS-induced senescent IMR90 cells using Human Genome U133 Plus 2.0 microarrays (Affymetrix) were obtained from the GEO database using accession nos. GSE40249 and GSE60652. RNA-normalized values were tested using the two-sample *t* test, with nominal p-values corrected for multiple testing using published procedures (Storey and Tibshirani, 2003). The false discovery rate of <15% threshold was used as a significance cutoff for differential gene expression. Genes shown in at least one dataset to be significantly up-regulated in senescent cells that had HMGB2 peaks with a significantly higher signal than in senescent versus control cells within 10 kb from the gene's transcription start site were considered direct HMGB2 targets. Significance of gene overlap selected from 17,833 unique microarray genes was estimated using the hypergeometrical test. Enrichment analysis was performed using DAVID software (National Institutes of Health; Huang et al., 2009), looking for gene ontology biological processes, molecular functions, and Swiss-Prot function keywords overrepresented among the genes regulated by HMGB2 in senescent cells. Only results with a false discovery rate of <5% were considered.

For analysis of H3K9me2/3 ChIP-Seq, data were downloaded from the GEO database (accession no. GSE38442), and reads were aligned to the human genome (version hg19) using Bowtie 2.2.5 (Langmead et al., 2009). ChIP-Seq enrichment was calculated using HOMER 4.7.2 (Heinz et al., 2010).

Prism version 5.0 (GraphPad Software) was used to perform statistical analyses. Unless otherwise indicated, *t* tests were used to determine p-values of raw data. A p-value of <0.05 was considered significant.

Online supplemental material

Fig. S1 is related to Fig. 1 and shows senescence markers for RAS-induced senescence and G4 *mTerc*$^{-/-}$ senescent cells. Additionally, Fig. S1 demonstrates that knockdown of HMGB2 induces senescence without affecting SASP gene expression. Fig. S2 is related to Fig. 2 and shows that HMGB1 does not bind to SASP gene loci and that HMGB2 binding to SASP gene loci is independent of both NF-κB and C/EBP-β. Fig. S3 is related to Figs. 3 and 4 and shows that knockdown or knockout of HMGB2 inhibits SASP gene expression in senescent cells and that knockdown or knockout of HMGB2 increases the heterochromatin marker H3K9me2 at SASP gene loci during senescence. Table S1 shows all primers used for qRT-PCR gene expression analysis. Table S2 shows all primers used for quantitative PCR of ChIP DNA. Table S3 is related to Fig. 1 and shows genes encoding chromatin regulatory proteins that were significantly altered in senescent cells across all four cross-referenced datasets. Table S4 is related to Fig. 2 and is the full enrichment analysis of genes regulated by HMGB2 in senescent cells performed using DAVID software.

Acknowledgments

The authors thank The Wistar Institute's Genomics, Bioinformatics, and Molecular Screening Facilities.

This work was supported by grants from the National Institutes of Health/National Cancer Institute (R01CA160331, R01CA163377, and R01CA202919 to R. Zhang; K99CA194309 to K.M. Aird; and K99CA194318 to B.G. Bitler), the Ovarian Cancer Research Fund program project (to R. Zhang), and the Jayne Koskinas and Ted Giovanis Breast Cancer Research Consortium at Wistar (to R. Zhang); by the subsidy of the Russian government to support the Program of Competitive Growth of Kazan Federal University (to N. Fatkhutdinov); and by the W.W. Smith Charitable Trust (grant C1501 to K. Noma). Support of core facilities used in this study was provided by Cancer Center Support Grant CA010815 to The Wistar Institute.

The authors declare no competing financial interests.

Submitted: 5 August 2016
Accepted: 21 September 2016

References

Acosta, J.C., A. O'Loghlen, A. Banito, M.V. Guijarro, A. Augert, S. Raguz, M. Fumagalli, M. Da Costa, C. Brown, N. Popov, et al. 2008. Chemokine signaling via the CXCR2 receptor reinforces senescence. *Cell.* 133:1006–1018. http://dx.doi.org/10.1016/j.cell.2008.03.038

Aird, K.M., G. Zhang, H. Li, Z. Tu, B.G. Bitler, A. Garipov, H. Wu, Z. Wei, S.N. Wagner, M. Herlyn, and R. Zhang. 2013. Suppression of nucleotide metabolism underlies the establishment and maintenance of oncogene-induced senescence. *Cell Reports.* 3:1252–1265. http://dx.doi.org/10.1016/j.celrep.2013.03.004

Aksoy, O., A. Chicas, T. Zeng, Z. Zhao, M. McCurrach, X. Wang, and S.W. Lowe. 2012. The atypical E2F family member E2F7 couples the p53 and RB pathways during cellular senescence. *Genes Dev.* 26:1546–1557. http://dx.doi.org/10.1101/gad.196238.112

Bianchi, M.E., and A. Agresti. 2005. HMG proteins: dynamic players in gene regulation and differentiation. *Curr. Opin. Genet. Dev.* 15:496–506. http://dx.doi.org/10.1016/j.gde.2005.08.007

Biniossek, M.L., A. Lechel, K.L. Rudolph, U.M. Martens, and S. Zimmermann. 2013. Quantitative proteomic profiling of tumor cell response to telomere dysfunction using isotope-coded protein labeling (ICPL) reveals interaction network of candidate senescence markers. *J. Proteomics.* 91:515–535. http://dx.doi.org/10.1016/j.jprot.2013.08.007

Campisi, J. 2013. Aging, cellular senescence, and cancer. *Annu. Rev. Physiol.* 75:685–705. http://dx.doi.org/10.1146/annurev-physiol-030212-183653

Campisi, J., J.K. Andersen, P. Kapahi, and S. Melov. 2011. Cellular senescence: a link between cancer and age-related degenerative disease? *Semin. Cancer Biol.* 21:354–359.

Chandra, T., and M. Narita. 2013. High-order chromatin structure and the epigenome in SAHFs. *Nucleus.* 4:23–28. http://dx.doi.org/10.4161/nucl.23189

Chandra, T., K. Kirschner, J.Y. Thuret, B.D. Pope, T. Ryba, S. Newman, K. Ahmed, S.A. Samarajiwa, R. Salama, T. Carroll, et al. 2012. Independence of repressive histone marks and chromatin compaction during senescent heterochromatic layer formation. *Mol. Cell.* 47:203–214. http://dx.doi.org/10.1016/j.molcel.2012.06.010

Chien, Y., C. Scuoppo, X. Wang, X. Fang, B. Balgley, J.E. Bolden, P. Premsrirut, W. Luo, A. Chicas, C.S. Lee, et al. 2011. Control of the senescence-associated secretory phenotype by NF-κB promotes senescence and enhances chemosensitivity. *Genes Dev.* 25:2125–2136. http://dx.doi.org/10.1101/gad.17276711

Childs, B.G., M. Durik, D.J. Baker, and J.M. van Deursen. 2015. Cellular senescence in aging and age-related disease: from mechanisms to therapy. *Nat. Med.* 21:1424–1435. http://dx.doi.org/10.1038/nm.4000

Coppé, J.P., P.Y. Desprez, A. Krtolica, and J. Campisi. 2010. The senescence-associated secretory phenotype: the dark side of tumor suppression. *Annu. Rev. Pathol.* 5:99–118. http://dx.doi.org/10.1146/annurev-pathol-121808-102144

Davalos, A.R., M. Kawahara, G.K. Malhotra, N. Schaum, J. Huang, U. Ved, C.M. Beausejour, J.P. Coppe, F. Rodier, and J. Campisi. 2013. p53-dependent release of Alarmin HMGB1 is a central mediator of senescent phenotypes. *J. Cell Biol.* 201:613–629. http://dx.doi.org/10.1083/jcb.201206006

Dimri, G.P., X. Lee, G. Basile, M. Acosta, G. Scott, C. Roskelley, E.E. Medrano, M. Linskens, I. Rubelj, O. Pereira-Smith, et al. 1995. A biomarker that identifies senescent human cells in culture and in aging skin in vivo. *Proc. Natl. Acad. Sci. USA.* 92:9363–9367. http://dx.doi.org/10.1073/pnas.92.20.9363

Du, X., J. Shen, N. Kugan, E.E. Furth, D.B. Lombard, C. Cheung, S. Pak, G. Luo, R.J. Pignolo, R.A. DePinho, et al. 2004. Telomere shortening exposes functions for the mouse Werner and Bloom syndrome genes. *Mol. Cell. Biol.* 24:8437–8446. http://dx.doi.org/10.1128/MCB.24.19.8437-8446.2004

Heinz, S., C. Benner, N. Spann, E. Bertolino, Y.C. Lin, P. Laslo, J.X. Cheng, C. Murre, H. Singh, and C.K. Glass. 2010. Simple combinations of lineage-determining transcription factors prime cis-regulatory elements required for macrophage and B cell identities. *Mol. Cell.* 38:576–589. http://dx.doi.org/10.1016/j.molcel.2010.05.004

Huang, W., B.T. Sherman, and R.A. Lempicki. 2009. Systematic and integrative analysis of large gene lists using DAVID bioinformatics resources. *Nat. Protoc.* 4:44–57. http://dx.doi.org/10.1038/nprot.2008.211

Kuilman, T., C. Michaloglou, L.C. Vredeveld, S. Douma, R. van Doorn, C.J. Desmet, L.A. Aarden, W.J. Mooi, and D.S. Peeper. 2008. Oncogene-induced senescence relayed by an interleukin-dependent inflammatory network. *Cell.* 133:1019–1031. http://dx.doi.org/10.1016/j.cell.2008.03.039

Langmead, B., C. Trapnell, M. Pop, and S.L. Salzberg. 2009. Ultrafast and memory-efficient alignment of short DNA sequences to the human genome. *Genome Biol.* 10. http://dx.doi.org/10.1186/gb-2009-10-3-r25

Li, H., Q. Cai, A.K. Godwin, and R. Zhang. 2010. Enhancer of zeste homolog 2 promotes the proliferation and invasion of epithelial ovarian cancer cells. *Mol. Cancer Res.* 8:1610–1618. http://dx.doi.org/10.1158/1541-7786.MCR-10-0398

Malarkey, C.S., and M.E. Churchill. 2012. The high mobility group box: the ultimate utility player of a cell. *Trends Biochem. Sci.* 37:553–562. http://dx.doi.org/10.1016/j.tibs.2012.09.003

Muñoz-Espín, D., and M. Serrano. 2014. Cellular senescence: from physiology to pathology. *Nat. Rev. Mol. Cell Biol.* 15:482–496. http://dx.doi.org/10.1038/nrm3823

Narita, M., S. Nũnez, E. Heard, M. Narita, A.W. Lin, S.A. Hearn, D.L. Spector, G.J. Hannon, and S.W. Lowe. 2003. Rb-mediated heterochromatin formation and silencing of E2F target genes during cellular senescence. *Cell.* 113:703–716. http://dx.doi.org/10.1016/S0092-8674(03)00401-X

Narita, M., A.R. Young, and M. Narita. 2009. Autophagy facilitates oncogene-induced senescence. *Autophagy.* 5:1046–1047. http://dx.doi.org/10.4161/auto.5.7.9444

Nelson, D.M., T. McBryan, J.C. Jeyapalan, J.M. Sedivy, and P.D. Adams. 2014. A comparison of oncogene-induced senescence and replicative senescence: implications for tumor suppression and aging. *Age (Dordr.).* 36:1049–1065. http://dx.doi.org/10.1007/s11357-014-9637-0

Pérez-Mancera, P.A., A.R. Young, and M. Narita. 2014. Inside and out: the activities of senescence in cancer. *Nat. Rev. Cancer.* 14:547–558. http://dx.doi.org/10.1038/nrc3773

Rudolph, K.L., S. Chang, H.W. Lee, M. Blasco, G.J. Gottlieb, C. Greider, and R.A. DePinho. 1999. Longevity, stress response, and cancer in aging telomerase-deficient mice. *Cell.* 96:701–712. http://dx.doi.org/10.1016/S0092-8674(00)80580-2

Sanjana, N.E., O. Shalem, and F. Zhang. 2014. Improved vectors and genome-wide libraries for CRISPR screening. *Nat. Methods.* 11:783–784. http://dx.doi.org/10.1038/nmeth.3047

Storey, J.D., and R. Tibshirani. 2003. Statistical significance for genomewide studies. *Proc. Natl. Acad. Sci. USA.* 100:9440–9445. http://dx.doi.org/10.1073/pnas.1530509100

Takebayashi, S., H. Tanaka, S. Hino, Y. Nakatsu, T. Igata, A. Sakamoto, M. Narita, and M. Nakao. 2015. Retinoblastoma protein promotes oxidative phosphorylation through upregulation of glycolytic genes in oncogene-induced senescent cells. *Aging Cell.* 14:689–697. http://dx.doi.org/10.1111/acel.12351

Thomas, J.O. 2001. HMG1 and 2: architectural DNA-binding proteins. *Biochem. Soc. Trans.* 29:395–401. http://dx.doi.org/10.1042/bst0290395

Tu, Z., K.M. Aird, B.G. Bitler, J.P. Nicodemus, N. Beeharry, B. Xia, T.J. Yen, and R. Zhang. 2011. Oncogenic RAS regulates BRIP1 expression to induce dissociation of BRCA1 from chromatin, inhibit DNA repair, and promote senescence. *Dev. Cell.* 21:1077–1091. http://dx.doi.org/10.1016/j.devcel.2011.10.010

van Deursen, J.M. 2014. The role of senescent cells in ageing. *Nature.* 509:439–446. http://dx.doi.org/10.1038/nature13193

Wiley, C.D., M.C. Velarde, P. Lecot, S. Liu, E.A. Sarnoski, A. Freund, K. Shirakawa, H.W. Lim, S.S. Davis, A. Ramanathan, et al. 2016. Mitochondrial dysfunction induces senescence with a distinct secretory phenotype. *Cell Metab.* 23:303–314. http://dx.doi.org/10.1016/j.cmet.2015.11.011

Ye, X., B. Zerlanko, A. Kennedy, G. Banumathy, R. Zhang, and P.D. Adams. 2007. Downregulation of Wnt signaling is a trigger for formation of facultative heterochromatin and onset of cell senescence in primary human cells. *Mol. Cell.* 27:183–196. http://dx.doi.org/10.1016/j.molcel.2007.05.034

Zhang, R., W. Chen, and P.D. Adams. 2007. Molecular dissection of formation of senescence-associated heterochromatin foci. *Mol. Cell. Biol.* 27:2343–2358. http://dx.doi.org/10.1128/MCB.02019-06